Maneuverability Assessment of a Compound Helicopter Configuration

Kevin Ferguson

Ph.D Student,

University of Glasgow,

James Watt South Building, Glasgow

Douglas Thomson

Senior Lecturer,

University of Glasgow,

James Watt South Building, Glasgow

Abstract

The compound helicopter design could potentially satisfy the new emerging requirements placed on the next generation of rotorcraft. The main benefit of the compound helicopter is its ability to reach speeds that significantly surpass the conventional helicopter. However, it is possible that the compound helicopter design can provide additional benefits in terms of maneuverability. The paper features a conventional helicopter and a compound helicopter. The conventional helicopter features a standard helicopter design with a main rotor providing the propulsive and lifting forces whereas a tail rotor, mounted at the rear of the aircraft, provides the yaw control. The compound helicopter configuration features both lift and thrust compounding. The wing offloads the main rotor at high speeds whereas two propellers provide additional axial thrust as well as yaw control. This study

Presented at the 40th European Rotorcraft Forum, Southampton, U.K., September 2-5th, 2014.

This manuscript has been submitted for consideration for publication in the Journal of the American Helicopter Society.

investigates the maneuverability of these two helicopter configurations using inverse simulation. The results predict that a compound helicopter configuration is capable of attaining greater load factors than its conventional counterpart, when flying a Pullup-Pushover maneuver. In terms of the Accel-Decel maneuver, the compound helicopter configuration is able of completing the maneuver in a shorter time than the conventional helicopter, but at the expense of greater installed engine power. The addition of thrust compounding to the compound helicopter design reduces the pitch attitude required throughout the acceleration stage of the maneuver.

Nomenclature

F_{prop}	propeller force in the x_e direction (N)
F_{tot}	total force required in the x_e direction (N)
F_{xe}, F_{ze}	force in the x_e and z_e directions (N)
g	acceleration due to gravity (m/s^2)
k	time point counter
L, M, N	external moments in the body axes set (Nm)
m	aircraft mass (kg)
n_{max}	maximum normal load factor
n_z	normal load factor
C_T/σ	main rotor blade loading
P_{tot}	engine power (kW)
R, R_{prop}	main rotor and propeller radius (m)
S	Accel-Decel distance (m)
t	time (s)
$\mathbf{u}$	control vector (rad)
V	aircraft flight speed (m/s)
$\dot{V}$	aircraft acceleration (m/s^2)
x, y, z	maneuver flight path co-ordinates (m)

$\mathbf{x}$	state vector (various units)
$\dot{x}, \dot{y}, \dot{z}$	earth axes velocities (m/s)
$\ddot{x}, \ddot{y}, \ddot{z}$	earth axes accelerations (m/s^2)
x_e, z_e	x and z directions of the Earth axes set
$\mathbf{x}_{prop}$	position vector of the two propeller hubs (m)
X, Y, Z	external forces in the body set (N)
$\mathbf{y}_{des}$	trajectory definition matrix (various units)
α_e	trimmed fuselage angle of attack (rad)
$\alpha^{'}$	fuselage angle of attack excursion (deg)
σ, σ_{prop}	main rotor and propeller solidity
θ_{tw}	main rotor or propeller twist gradient (deg)
χ	track angle (rad)
γ	glideslope angle (rad)
γ_{rot}	Lock number
$\dot{\gamma}$	time derivative of the glideslope angle (rad/s)
Ω, Ω_{prop}	main rotor and propeller rotational speeds (rad/s)
Φ, Θ, Ψ	Euler angles (deg)
θ_0	main rotor collective pitch angle (deg)
θ_{1s}	main rotor longitudinal pitch angle (deg)
θ_{1c}	main rotor lateral pitch angle (deg)
θ_{diff}	propellers differential control pitch angle (deg)
$\bar{\theta}_{prop}$	mean propeller pitch angle (deg)

Introduction

The compound helicopter has experienced a resurgence of interest due to its ability to obtain speeds that significantly surpass the conventional helicopter. This increase in speed, provided that efficient hover capability is maintained, would make the compound helicopter suitable for various roles and missions such

as troop insertion, search and rescue, ship replenishment as well as short haul flights in the civil market. The compounding of a helicopter is not a new idea but the development of a compound helicopter has proven elusive for the rotorcraft community due to a combination of technical problems and economical issues [1]. The rotorcraft community is again exploring the compound helicopter design, with various manufacturers testing their prototypes.

The success of the conventional helicopter is partly due to its unique ability to perform precise maneuvers in Nap of the Earth (NoE) flight. One method of assessing the helicopter's ability to perform maneuvers is inverse simulation. Inverse simulation reverses the conventional simulation approach by calculating the control activity required to force a vehicle along a particular trajectory [2]. The first inverse simulation algorithm, known as the differentiation method, was developed by Thomson and Bradley [3] to assess the agility of a helicopter using a six degree of freedom (DOF) rotorcraft model. The success of the inverse simulation results, as well as the increasing interest in handling qualities and pilot workload research, prompted future development of the algorithm. Subsequently, inverse simulation has been used for various applications, including investigating pilot control strategies, conceptual design analyses and handling qualities [4–7]. Despite the success of the differentiation method, there were some problems which consequently led to a new approach to inverse simulation. The major limitation of the differentiation method was that the mathematical model and the algorithm were strongly coupled, therefore even slight changes to the mathematical model required alterations to the algorithm itself. Realizing this shortcoming, Hess, Goa and Wang developed a generalized technique of inverse simulation [8], often referred to as the integration method, which fully separates the mathematical model from the algorithm. Due to the robust and flexible nature of this technique, the integration method has become the most common approach [9].

Before proceeding, other methods of solving the inverse problem should be noted. Firstly, is the two time-scale method which was developed by Avanzini, de Matteis and de Socio [10, 11]. This method assumes that the rotational dynamics of an aircraft are much quicker than the translational dynamics, therefore permitting the assumption that the main rotor collective controls the translational dynamics whereas the cyclic and pedals influence the rotational dynamics. This method, similar to the other methods, use iterative schemes, such as the Newton-Raphson method, in order to solve the inverse problem.

However, the Newton-Raphson method can be replaced with an optimization algorithm to calculate the control angles, with Celi and de Matteis et al. [12, 13] successfully implementing optimization algorithms in their respective approaches. The optimization approach to inverse simulation is particularly useful to problems featuring control redundancy, however an appropriate cost function must be formed. Another method which could be used to calculate the appropriate control time histories is an inverse method using Adaptive Neural Networks (ANN). This approach has been used successfully in various rotorcraft control studies [14–19]. With this approach, the control action that is required is calculated by dynamic model inversion, which has proven to be a popular feedback linearization technique [20]. However, the major disadvantage of this technique is the significant errors that occur between the predicted and actual response of the aircraft due to inaccuracies within the plant model. As neural networks have the ability to accurately predict nonlinear functions [21], ANN can be used to atone for these errors. Although dynamic inversion techniques using ANN have considerable merit, the integration method of inverse simulation is used within this study due to its robust and flexible nature.

Maneuverability is an important design feature if the helicopter is to operate in tight Nap of the Earth (NoE) scenarios [22]. The ability of the helicopter to maneuver quickly and effectively enables the vehicle to quickly re-position. Furthermore, enhancing the maneuverability and agility of a helicopter can also aid its survivability with its ability to quickly turn or climb to avoid an attack. Traditionally, the design process has focused on performance and cost to drive the design of the helicopter. However, for the reasons previously stated, a high level of maneuverability has become a key design goal for most designers as it increases mission effectiveness [23]. As there is a demand for conventional helicopters to be maneuverable, it is reasonable to expect that operators would expect the same for a compound helicopter. Therefore, this paper presents a maneuverability assessment of a compound helicopter and compares the results to a conventional helicopter of similar shape and mass. Before proceeding, it is important to highlight that there are various definitions of the term maneuverability. Therefore it is necessary to define what is meant by maneuverability in this current work. Generally, most authors agree that maneuverability is the ability of the aircraft to change its flight path [22,24] with Whalley [25] providing an overview of the various definitions proposed by authors. Whalley also concludes by stating his definition of maneuverability, which is the following

"Maneuverability is the measure of the maximum achievable time-rate-of-change of velocity vector at any point in the flight envelope."

The aim of the current work is to determine the maximum maneuvering capability of two aircraft configurations, namely a conventional helicopter configuration and a compound helicopter configuration, then to subsequently investigate if the compounding of the conventional helicopter offers an advantage in this regard. Hence, in this context, the term "maneuverability" and phrase "maximum maneuvering capability" are used interchangeably throughout the remainder of this paper. Although not the primary aim of the study, due to the use of inverse simulation, the results from the work are likely to highlight some of the potential control actions that a pilot may use to fly a compound helicopter along a predetermined flight path. The strategy for the current work is to use an established mathematical model of a conventional helicopter (in this case, the AgustaWestland Lynx, as seen in Figure 1(a)), and then convert this model to represent a compound helicopter configuration. The Lynx is referred to as the baseline (BL) configuration throughout the paper and was chosen as the starting point as a well established dataset was available [26]. Another reason for the choice of the Lynx is that it features a rigid rotor which is likely to be used in a compound helicopter design [27]. One primary advantage of the rigid rotor is its ability to generate powerful moments independent of the amount of rotor thrust. This feature is particularly suited to a winged compound helicopter design as the wing offloads the main rotor in high speed flight. Therefore, the application of a rigid rotor would allow the aircraft to be controlled, by the main rotor, despite the low levels of rotor loading expected in high speed flight [28]. The compound configuration that is examined in the paper is broadly similar to the Eurocopter X^3 with the preliminary design of the configuration discussed in a previous compound helicopter study [29]. This configuration is named the compound helicopter (CH) configuration, which features a wing and two propellers, as seen in Figure 1(b). This compound helicopter configuration is changed as little as possible, relative to the baseline configuration, to allow for a fair and direct comparison between the results of the two configurations. The result is a rather unusual looking vehicle, Figure 1(b); however, it should be stressed that this is not a design exercise but a study to investigate the influence of compounding. Therefore to ensure that the effects of compounding are isolated from other factors, the basic vehicle shape and size is maintained. The approach in this work is to use

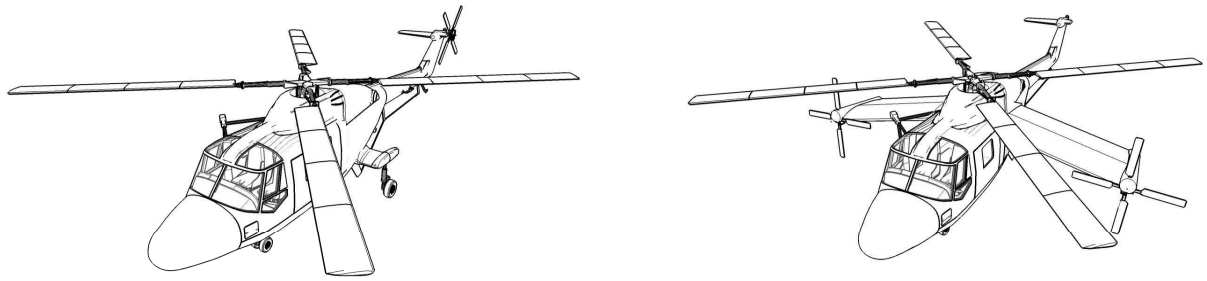

(a) Baseline Helicopter (b) Compound Helicopter

Fig. 1 Sketches of the two Helicopter Configurations

inverse simulation to quantify the maneuverability of the aircraft configurations. This requires various elements such as helicopter mathematical models, an inverse simulation algorithm, modeling of helicopter maneuvers and a maneuverability assessment method. The following section provides an overview of these required components.

Methodology

Helicopter Mathematical Modeling

The conventional and compound helicopter models are developed using the Helicopter Generic Simulation (HGS) model [30]. The HGS model is a conventional disk-type rotorcraft model, as described by Padfield [26], and has found extensive use in studies of helicopter flight dynamics. The HGS model is generic in structure with only the helicopter's parameters required to model the vehicle. The main rotor model, within the HGS package, ignores the pitching and lagging degrees of freedom, therefore assuming that the flap dynamics have the most influence in terms of the helicopter's flight dynamic characteristics. The flapping dynamics are assumed to be quasi steady, a common assumption in main rotor modeling, therefore permitting a multi-blade representation of the main rotor. The rotor model neglects the rotor periodicity by assuming that only the steady components of the periodic forces and moments generated by the main rotor influence the helicopter's body dynamics. The main rotor is assumed to be centrally hinged with stiffness in flap and with the main rotor chord assumed to be constant. Furthermore, the model also features a dynamic inflow and a rotor-speed governor model. One important assumption, within the

rotor model, is that the aerodynamics are linear, so that the lift is a linear function of the local blade angle of attack, whereas the drag is modeled by a simple polynomial. Due to this assumption, nonlinear aerodynamics such as retreating blade stall and compressibility are not modeled. To model the nonlinear aerodynamics and rotor periodicity requires an "individual blade model", examples of which are given by Kim et.al, Rutherford, Mansur and Houston [31–34]. Regarding the modeling of the other subsystems of the rotorcraft, the forces and moments of the tailplane, fuselage, and fin are calculated using a series of lookup tables derived from experimental data [26].

One question that naturally arises is the validity of these models and if the results from these rotorcraft models would replicate the real aircraft. In terms of the conventional helicopter, inverse simulation results have shown good correlation for a range of maneuvers [35], giving confidence to the worth of the results produced by the HGS model. In relation to the compound helicopter model, a strict validation based on the comparison of flight test with simulation results is not possible, as the appropriate data is not yet openly available. The assumption in this work is that a well-established mathematical model, coupled with validated propeller and wing models will reasonably represent the compound helicopter. The limitations of the main rotor model used in this work are well understood [26] and include the inability to accurately capture off-axis effects and low fidelity at the edges of the flight envelope where, for example, the aerodynamics are highly nonlinear. Despite these model features, this model was selected for three primary reasons. Firstly, by reviewing the literature, many of the mathematical models used in inverse simulation studies do not reach the level 1 category of Padfield's threefold hierarchy of rotor simulation levels [26]. For example, Hess and Gao [9] have used linear derivatives for calculating the main rotor's forces and moments. In addition, inverse simulation has been used by Whalley [25] to predict the maximum maneuvering capability of helicopter configurations. In that particular study, Whalley used a linear model to predict the maneuverability of the vehicle which included a successful validation of the inverse simulation results through a series of piloted simulation experiments. In the context of this present study, the authors have decided to use the nonlinear HGS model which is a well-established helicopter model which falls firmly within the level 1 category of simulation models. The level of modeling used within this study seems appropriate given that other inverse simulation studies have used some rather simplistic linear models. The modeling in this study is not as basic as many of these linear models described in

the literature but neither is it detailed as the modeling featured in some comprehensive rotorcraft codes. Hence, the modeling used in this work can perhaps be described as a reasonable compromise between the two extremes of the modeling scales. The second reason for the choice of the HGS model is that a high-fidelity mathematical model would require significant computational effort. A comprehensive helicopter model, coupled with the inverse simulation algorithm would result in simulations that would take weeks, if not months, to run. In contrast, inverse simulation results with the HGS model can be obtained within minutes. The last reason for the choice of the HGS model, is that a high level helicopter model would inevitably introduce new numerical and stability issues to the inverse simulation algorithm. To date, there is no comprehensive explanation why some of these numerical issues arise [36]. As the focus of the study is not to develop a new inverse simulation algorithm, it seems appropriate to use the existing HGS model where numerical instabilities can be avoided by careful selection of the inputs to the inverse simulation algorithm.

The HGS package is configured to represent the two aircraft configurations featured in this study. As mentioned previously, the conventional helicopter is based on the AgustaWestland Lynx with Table 1

Table 1. Configuration data for the BL and CH configurations

Design Parameter	BL and CH Configurations
R (m)	6.4
Ω (rad/s)	35.6
θ_{tw} (deg)	-8
σ	0.077
γ_{rot}	7.12
m (kg)	4313

providing some of the important configuration data [26]. Recall that this is not a design exercise, where the compound helicopter's powerplant and weight are sized to fulfill a particular mission, but a study to examine the effects of compounding to the maneuverability of the helicopter. Hence, to isolate the effects of compounding from other factors, the design changes between the BL and CH configurations are solely due to compounding. As a consequence, the main rotor design of the CH helicopter is identical to that of the BL configuration, as described in Table 1. In terms of the CH configuration it is necessary to size the propellers and wing. The wing must be sized in a manner that does not adversely reduce hover performance, as the wing is likely to create a significant download in the hover, while having the ability to offload the main rotor at high speeds. Another complication is that the sizing of the wing influences the design of the propellers. With this design, the propellers are required to provide the anti-torque moment in low-speed flight. The propellers are mounted on the outer sections of the wing to provide adequate clearance between the propeller blades and the fuselage. It is clear that a greater wingspan will result in lower propeller thrusts required to provide the anti-torque moment as the lever arm from the propeller to the center of mass is increased. The selected wing area for the CH configuration is 12m^2 with an aspect ratio of 6. This wing area can create a significant amount of lift at high speed without adversely degrading hover performance. Also, this combination of the wing area and aspect ratio creates a sizable lever arm between the propellers and the center of mass, thus reducing the propeller thrusts at low-speed flight. In terms of the aspect ratio, a value of 6 is chosen because a higher aspect ratio would lead to a wingspan that would extend further into the higher velocities of the rotor wake, whereas a lower aspect ratio would result in a greater induced drag penalty [37]. A choice of 6 is an appropriate compromise between these two effects and has been used on various winged helicopters [38, 39]. Regarding the design of the propellers, Table 2 shows the chosen design parameters of the propellers. The rotational speed is chosen to provide high-velocity airflow over the propeller blades without compressibility effects becoming an issue in high speed flight. The propeller also features Clark Y airfoils, which are typically used in propellers, with a high level of twist so that each propeller blade element operates at a favorable angle of attack [40].

Table 2. Propeller Data

Design Parameter	CH Configuration
R (m)	1.3
Ω_{prop} (rad/s)	207
θ_{tw} (deg)	-30
σ_{prop}	0.193
$\mathbf{x}_{prop}$ (m)	$(0.05, \pm 3.87, 0.13)$

Inverse Simulation Algorithm

The inverse simulation algorithm used in this current study is the so called integration method. As this method is well documented in the literature [2, 9, 41] only a brief description is provided within. The integration method uses numerical integration and conventional simulation to calculate the controls required to move a vehicle through a desired trajectory. The first step is to calculate the control angles that trim the aircraft for the given starting flight speed. Generally, a helicopter can be in trimmed flight when climbing, descending or flying with a lateral velocity (sideslip). However in this current work the trimmed state corresponds to steady level flight with the body accelerations and the attitude rates equal to zero. Concerning the BL configuration, the trim algorithm calculates the four control angles, roll and pitch angles which result in zero translational and angular accelerations acting at the aircraft's center of gravity. Essentially, there are six trim targets which are

$$X - mg\sin\Theta \tag{1}$$

$$Y + mg\cos\Theta\sin\Phi \tag{2}$$

$$Z + mg\cos\Theta\cos\Phi \tag{3}$$

$$L = 0 \tag{4}$$

$$M = 0 \tag{5}$$

$$N = 0 \tag{6}$$

which correspond to the condition of steady level flight. However, the introduction of an extra control(s) to the CH configuration requires a slight amendment to the trim algorithm. The CH configuration features five controls: the main rotor collective, two cyclic controls, a mean propeller pitch control and a differential propeller pitch control. The approach taken to determine the control angles required to trim this aircraft configuration is to prescribe an additional state which results in six unknowns which match the six trim targets, Equations (1) - (6). Presently, the extra state which is prescribed is the pitch attitude, Θ, as it directly impacts the level of thrust that the propellers are required to produce. One possibility is to set a fixed value of pitch to trim the helicopter at all flight speeds; for example, $\Theta = 0$, fuselage level. However, this is not always desirable, as it would require excessive levels of propeller thrusts at certain flight speeds. Another concern is that, in low-speed flight, there is no distinct advantage of having the propellers providing significant amounts of thrust, as it would unnecessarily increase the overall power consumption of the helicopter. Hence, rather than setting the pitch attitude to a fixed value for all flight speeds, a pitch schedule is developed. In low speed flight, the pitch schedule results in small amounts of propeller thrusts to provide the anti-torque moment. Whereas in speeds in excess of 150 kt, the pitch attitude is scheduled so that the wing's lift coefficient, C_L, is approximately 0.5. This results in the wing providing a significant amount of lifting force whilst retaining an adequate stall margin. A consequence of this trim approach is that the two propellers provide the majority of propulsive force to overcome the airframe drag in high speed flight.

The next step, after the calculation of the trim control angles, is to define the maneuver. The maneuver

is discretized into a series of discrete time points, t_k, by specifying the time step. Subsequently, the maneuver can be determined with a matrix, $\mathbf{y}_{des}(t_k)$ representing the flight path of the maneuver. The maneuver can be defined by polynomials that satisfy the requirements of the particular maneuver [42], with the mathematical modeling of these maneuvers detailed later. Starting from the trimmed condition, $\mathbf{u}_e$ is the initial guess to calculate the control vector, $\mathbf{u}$, to force the helicopter to the position of the next time point. A Newton-Raphson technique is used to calculate the control vector to force the vehicle to the next time point to match the desired flight path defined by $\mathbf{y}_{des}(t_k)$. After convergence, this numerical technique moves onto the next time point and repeats the process. The end result is the control activity required throughout the maneuver.

ADS-33 Maneuver Modeling

ADS-33 Pullup-Pushover Maneuver

Of course, to successfully implement inverse simulation, the trajectory the aircraft is to follow is required. In the early inverse simulation algorithms, the output vector, which describes the trajectory, was defined as follows:

$$\mathbf{y}_{des} = [x_e \quad y_e \quad z_e \quad \Psi]^T \tag{7}$$

where x_e, y_e and z_e are the flight path co-ordinates and the additional constraint, Ψ, is the heading angle. However with this form of output vector the calculated control activity contained high frequency oscillations [2]. By modifying the output vector to the following:

$$\mathbf{y}_{des} = [\ddot{x}_e \quad \ddot{y}_e \quad \ddot{z}_e \quad \dot{\Psi}]^T \tag{8}$$

was shown to attenuate these oscillations [32]. Therefore, in this current work the output vector consists of the aircraft accelerations and heading rate. The accelerations are determined by the differentiation of the velocities in Earth axes, which are given by:

$$\dot{x} = V\cos\gamma\cos\chi \tag{9}$$

$$\dot{y} = V\cos\gamma\sin\chi \tag{10}$$

$$\dot{z} = -V\sin\gamma \tag{11}$$

leading to the following accelerations:

$$\ddot{x} = \dot{V}\cos\gamma\cos\chi - V\dot{\gamma}\sin\gamma\cos\chi - V\dot{\chi}\cos\gamma\sin\chi \tag{12}$$

$$\ddot{y} = \dot{V}\cos\gamma\sin\chi - V\dot{\gamma}\sin\gamma\sin\chi + V\dot{\chi}\cos\gamma\cos\chi \tag{13}$$

$$\ddot{z} = -\dot{V}\sin\gamma - V\dot{\gamma}\cos\gamma \tag{14}$$

It is therefore clear that if the flight speed and trajectory angle profiles are known then the accelerations in the Earth axes set can be determined. In contrast, if expressions of x_e, y_e and z_e as a function of time are available then the accelerations can be determined easily without the use of Equation (12)- (14). However, the general case is that the accelerations can be obtained by specifying the flight speed and trajectory angles throughout the maneuver.

The maneuvers studied within this paper are typical conventional helicopter maneuvers, similar to the Pullup-Pushover and Accel-Decel maneuvers described in the ADS-33 requirements [43]. Although the introduction of compounding to the helicopter is likely to expand the operational flight envelope of the vehicle, a compound helicopter will still spend a significant amount of time operating in conventional helicopter flight regimes. As a consequence, it is important to understand and quantify the compound helicopter's ability to perform typical maneuvers which conventional helicopters routinely complete. The Pullup-Pushover maneuver involves the aircraft achieving positive and negative load factors. The objective of the Pullup-Pushover maneuver, as described in ADS-33 [43], is to examine the ability of the aircraft to avoid obstacles during high speed NoE operations. The aircraft begins the maneuver at a trimmed condition at a flight speed equal to or less than 120 kt. In the pullup stage of the maneuver the aircraft is required to achieve a positive normal load factor and maintain this for a given period of time. Following this the aircraft is then to transition to a pushover and achieve a negative load factor then to recover to level

flight as quickly as possible. The normal load factor is a measure of vertical acceleration and is defined as

$$n_z = 1 - \frac{\ddot{z}}{g} \tag{15}$$

The rearrangement of Equation (11) gives the standard definition of the glideslope angle

$$\gamma = -\sin^{-1}\frac{\dot{z}}{V} \tag{16}$$

The time derivative of the glideslope angle is therefore

$$\dot{\gamma} = \frac{-\ddot{z}V + \dot{V}\dot{z}}{V^2\cos\gamma} \tag{17}$$

Through the use of Equations (15) and (17), the time derivative of the glideslope angle can be expressed in terms of the normal load factor and flight speed as

$$\dot{\gamma} = \frac{\dot{V}\dot{z} - V(g - gn_z)}{V^2\cos\gamma} \tag{18}$$

The next step is to define the load factor distribution throughout the maneuver by applying the maneuver boundary conditions. The ADS-33 document specifies the majority of the load factors to be attained throughout the maneuver [43]. To meet the desired standards of this maneuver, the maximum positive load factor must be attained after 1s of commencing the maneuver and sustained for a further 2s. Thereafter, the helicopter transitions from the positive load factor to the lowest load factor within 2s, and maintains this load factor for a further 2s. Figure 2 shows a typical load factor distribution which relates to the desirable standards set in the specification. The specification does not explicitly define an end time of the maneuver, a point raised by Celi [44], but does state that after the pushover stage of the maneuver the aircraft should "*recover to level flight as rapidly as possible*". The assumption in this current work is that the maneuver ends when the aircraft's original flight speed is recovered at $t = t_5$ with the normal load factor returning to unity and sustained at this value for a further 2s until $t = t_6$. The approach taken to form the load factor distribution across the maneuver is to split the maneuver into six sections and apply maneuver boundary conditions, as seen in Table 3, between each of the maneuver segments. In each of

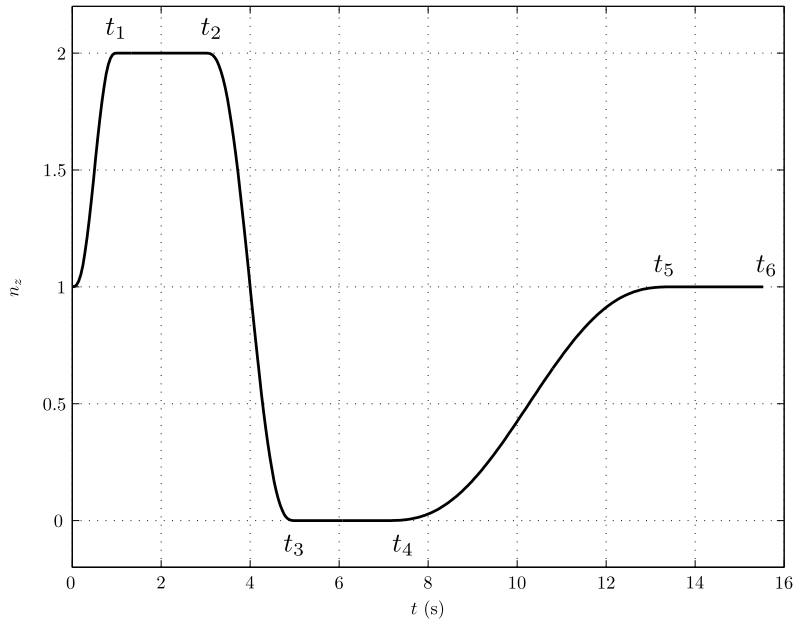

Fig. 2 Desirable Load Factor throughout the Pullup-Pushover maneuver.

the six segments, a fifth-order polynomial is formed to describe the load factor distribution. For example, between time t_0 and t_1, the load factor is given by:

$$n_z = a_0 t^5 + a_1 t^4 + a_2 t^3 + a_3 t^2 + a_4 t + a_5 \tag{19}$$

where the coefficients, a_0, a_1, a_2, a_3, a_4 and a_5, are determined by applying the boundary conditions be-

Table 3. Load Factor Boundary Conditions

Variable	$t_0 = 0s$	$t = t_1$	$t = t_2$	$t = t_3$	$t = t_4$	$t = t_5$	$t = t_6$
n_z	1	n_{max}	n_{max}	n_{min}	n_{min}	1	1
$\dot{n}_z$	0	0	0	0	0	0	0
$\ddot{n}_z$	0	0	0	0	0	0	0
α	α_e	$\alpha_e + \alpha'$	$\alpha_e + \alpha'$	$\alpha_e - \alpha'$	$\alpha_e - \alpha'$	α_e	α_e

tween time t_0 and t_1, so that the normal load factor distribution in this maneuver segment is known. The end result is that there are six fifth-order piecewise continuous polynomials which are similar to Equation (19). Each of these polynomials join at their endpoints with matching displacement and slope. These six polynomials are then pieced together so that the load factor distribution across the maneuver is known. The next step is to determine the variation of flight speed throughout the maneuver. One solution to this is to impose a predetermined profile of flight speed throughout the maneuver, however there is very little information regarding the variation of airspeed throughout this maneuver. The approach taken in this present work, in order to determine a flight speed profile, is to assume that there is a balance of potential and kinetic energy during the maneuver. For example, when the aircraft climbs there is a gain in potential energy which is balanced by a loss of kinetic energy. This assumption of the balance of energy leads to the following equation

$$\dot{V} = -g \sin \gamma \tag{20}$$

The result is that as the aircraft climbs airspeed reduces whereas as the vehicle descends then airspeed increases. There are now two differential equations, Equations (18) and (20), which can be integrated to determine the flight velocity and climb angle throughout the maneuver, using the initial trimmed conditions. As the track angle, χ, is set to zero since it is a longitudinal maneuver, using the calculated values of V, $\dot{V}$, γ and $\dot{\gamma}$ the accelerations in the Earth axes set can be determined. Recall that the time derivative of the heading angle, $\dot{\Psi}$, is constrained throughout the maneuver and set to zero.

As previously discussed, $\mathbf{y}_{des}$ is composed of the accelerations of $\ddot{x}_e$, $\ddot{y}_e$ and $\ddot{z}_e$ relative to the Earth axes set. Generally, the amount of inputs must match the number of outputs to find a unique solution. Therefore, since the conventional helicopter features four controls then the condition of zero heading or sideslip is included so that the output vector contains four elements. However, the 5 controls of the CH configuration presents an issue in order to calculate a unique solution of the control vector at each time point. One solution is to include an additional constraint in the output vector to match the 5 controls of the compound helicopter configuration. In terms of the Pullup-Pushover maneuver, the extra constraint is selected to be the time derivative of the fuselage angle of attack, $\dot{\alpha}$. An alternative approach could have

been to schedule a control such as θ_{1s} throughout the maneuver. However, the justification of the inclusion of an additional constraint with scheduling $\dot{\alpha}$ across the maneuver is that it is likely a pilot would adopt a control strategy which attempts to exploit the lifting capability of the wing in the pullup stage of the maneuver. It is found by experimentation that including $\dot{\alpha}$ as an additional constraint and appropriately scheduling this value over the duration of the maneuver results in the wing's angle of attack increasing and decreasing in the respective pullup and pushover stages of the maneuver. Table 3 shows the distribution of the fuselage angle of attack, starting at its trim value of α_e before increasing to a value of $\alpha_0 + \alpha^{'}$. This increase of the fuselage angle of attack in the pullup stage of the maneuver increases the wing's angle of attack helping the vehicle create a positive load factor. Similarly in the pushover stage of the maneuver the wing helps create a negative load factor. The value of $\alpha^{'}$ is taken to be 14° in the current work which results in the wing's angle of attack increasing significantly in the climbing stage of the maneuver. The fuselage angle of attack variation is described by a series of piecewise fifth order polynomials, similar in form to Equation 19, therefore the fuselage angle of attack time derivative, $\dot{\alpha}$, is easily obtained through differentiation.

ADS-33 Accel-Decel Maneuver

The Accel-Decel maneuver starts with the aircraft in the hover. It then accelerates to a flight velocity of 50 kt before aggressively decelerating back to a stabilized hover. The objective of this maneuver is to examine the pitch and heave axis handling qualities [43]. As the initial heading of the aircraft is to be maintained throughout the maneuver, the track angle, χ, and heading rate, $\dot{\Psi}$ are set to zero. The five boundary conditions of this maneuver are given in Table 4 with the assumption that the maximum flight velocity of 50 kt is reached at the half-way point. A fourth-order polynomial describes the flight velocity

$$V(t) = b_0 t^4 + b_1 t^3 + b_2 t^2 + b_3 t + b_4 \tag{21}$$

where b_0, b_1, b_2, b_3 and b_4 are coefficients which are determined by applying the boundary conditions. For this particular maneuver, $\dot{x} = V(t)$ whereas $\dot{y} = \dot{z} = 0$. The rate of change of the flight velocity is readily available through the differentiation of Equation (21), therefore allowing the calculation of the

Table 4. The Boundary Conditions of the Accel-Decel Maneuver.

Variable	$t = 0s$	$t = t_{end}/2$	$t = t_{end}$
V	0	50 kt	0
$\dot{V}$	0	0	0

accelerations which are contained in the output vector, $\mathbf{y}_{des}$. The maneuver is defined by setting the distance to be traveled, S, obtained by integration of Equation (21) rather than specifying t_{end}.

The approach taken to calculate the control activity of the CH configuration throughout the Accel-Decel maneuver is to add an additional constraint, so that there are five constraints which match the five unknown controls. A logical question which arises with the CH configuration flying an Accel-Decel maneuver is how much of the propulsive force is provided by the two propellers. Conveniently, the fifth constraint for the Accel-Decel maneuver is selected to be the ratio between the propeller's propulsive force (i.e. the force in the x_e direction) and the total propulsive force required. It is likely that in the acceleration phase of the maneuver that the pilot would adopt a control strategy which would actively use the two propellers to provide the propulsive force. As a result, it is assumed that the two propellers provide 75% of the total force in the x_e direction at the point of maximum forward acceleration which is approximately $t_{end}/4$, Figure 3. Note that the entire propulsive force could be provided by the thrust of the propellers alone, however simulation runs showed that this strategy increases the power of the total vehicle excessively. The percentage of 75% is not an optimal value, however it is a compromise between fully exploiting the propulsive force of the propellers whilst keeping the power requirements, in the acceleration phase of the maneuver, within realistic values. An additional advantage of thrust compounding is the possibility of using the propellers to decelerate the aircraft by providing reverse thrust. It is fair to assume that the design of the two propellers would be optimized for high speed flight

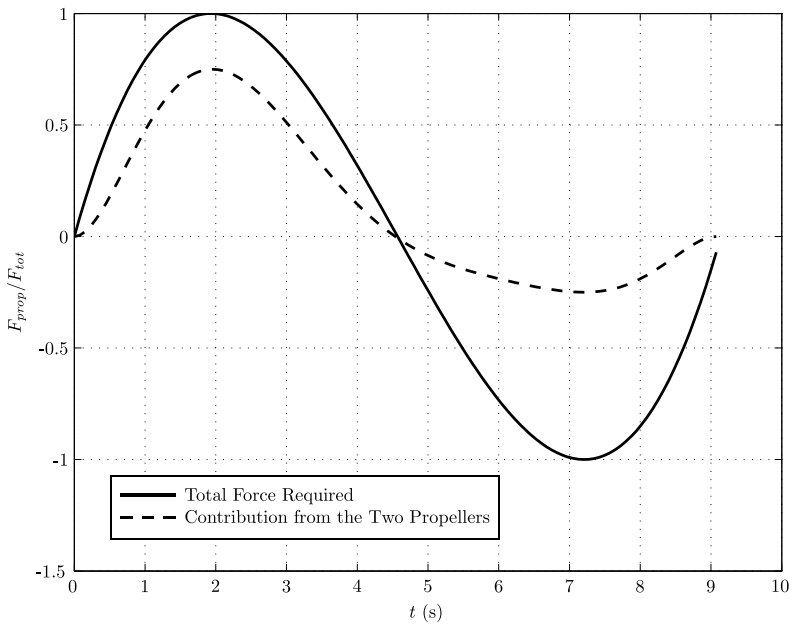

Fig. 3 Contribution of the two propellers to F_{xe} throughout the Accel-Decel maneuver.

and not for reverse thrust purposes where the propellers operate in the windmill brake state. Hence it is assumed that the propellers provide 25% of the entire reverse force required to decelerate the vehicle at the time of peak deceleration, $t \approx 3t_{end}/4$, as seen in Figure 3. The end result is that the majority of the propulsive force in the acceleration phase is provided by the thrust of the two propellers, whereas the deceleration phase involves more traditional helicopter like maneuvering. The ratio of the propeller's propulsive force (i.e. the force in the x_e direction) and total propulsive force required is dependent on time, Figure 3, and is formed by the use of a eighth order polynomial

$$\frac{F_{prop}}{F_{tot}} = c_0 t^8 + c_1 t^7 \ldots c_7 t + c_8 \tag{22}$$

where c_0, c_1, etc. are coefficients. The maneuver is now fully described by five constraints: three accelerations, heading rate and the thrust the propellers are required to produce. These five constraints match the five unknown controls, which the inverse simulation algorithm calculates. In this study, the pilot is actively using five controls which would undoubtedly increase the pilot workload throughout the maneuver. A solution to this issue could be a control system and interface, whereby the pilot has four available controls with a control system automatically altering the propeller pitch to increase propeller thrust in the

acceleration segment of the maneuver. Such an investigation is not considered in the current work, but will have to be examined in future studies, with the assumption made that the pilot can actively use all five controls simultaneously.

Maneuverability of the Configurations

The inverse simulation technique has been used to assess both the maneuverability and agility of helicopters [25, 45]. In this current work, a similar approach to Whalley's is adopted [25], in order to assess the maximum maneuvering capability of two helicopter configurations. However, there are some differences. Firstly, the integration method is used within this work unlike the differentiation technique used by Whalley [25]. The integration method has proven to be a robust and flexible approach which separates the mathematical model and the inverse simulation algorithm. This method also permits the inclusion of high fidelity modeling techniques, such as individual rotor blade modeling, which are not included within this study of compound helicopters but could be in future work.

Another important difference between Whalley's work and the current approach is the definition of the limiting factor which determines the aircraft's ability to complete a maneuver. There are various limits which define the maneuverability of a rotorcraft, which include aerodynamic, power and control travel limits [46]. In Whalley's work [25] it is assumed that the maximum or minimum control angles are the limiting factor for the helicopter configuration to perform a particular maneuver. Indeed this can be selected to be maneuverability limit in this work, however due to the assumption of linear aerodynamics within the current rotor model, and therefore not modeling blade stalling, the extreme limit of the main rotor collective can be reached producing an unrealistic amount of rotor thrust. The first solution to this is to assume that the aerodynamic limitations of the main rotor determine the maximum maneuvering capability of the vehicle. Hence, it is assumed that the limiting factor of certain maneuvers occurs when the main rotor blade loading, C_T/σ, reaches a maximum value. For transient maneuvers, such as pullups and turns, rotor blade stalling occurs at greater blade loading values than when compared to the helicopter in steady level flight [47]. This result has been confirmed by flight test data, see Figure 4, which was obtained from Lappos and Padfield [48]. The reason that the main rotor is able to delay the onset of

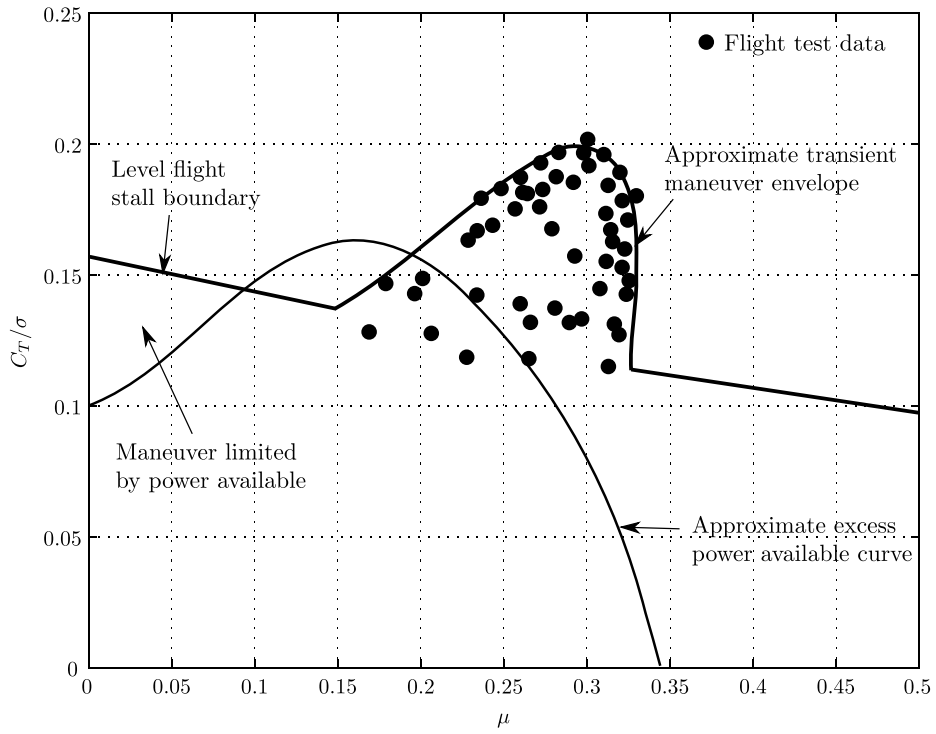

Fig. 4 Maneuver capability adapted from Lappos and Padfield [48]

retreating blade stall is due to the positive influence of the maneuver which effectively reduces the local angles of attack across the retreating side of the disk [47]. The flight test data obtained by Lappos and Padfield [48] can be conveniently used to approximate a transient maneuver boundary envelope, as seen in Figure 4. As this envelope has been established from flight test data, in the context of this study it is assumed that the limiting factor of certain maneuvers occurs when the main rotor's blade loading reaches the transient maneuver boundary in Figure 4. This limitation is appropriate in forward flight maneuvers due to the high levels of excess power available. However, for low speeds maneuvers, the maneuvering capability is generally limited by excess power available [46], as seen in Figure 4. Therefore, in low speed maneuvers it is appropriate to assume that the power available restricts the vehicle's ability to complete a maneuver. It is evident that the maneuverability limit could be due to the aerodynamic restrictions of the main rotor or power requirements. For these reasons, the maneuverability method allows the user to select their assumed limit which can be based on control travel limits, main rotor aerodynamic restrictions or the power available.

Figure 5 presents an overview of the Maneuverability Assessment Method (MAM). This iterative

method uses inverse simulation to determine the maximum maneuvering capability of the two aircraft configurations. The method begins at the first iterative counter and subsequently defines the maneuver. Thereafter, the integration method calculates the control angles required to force the particular aircraft

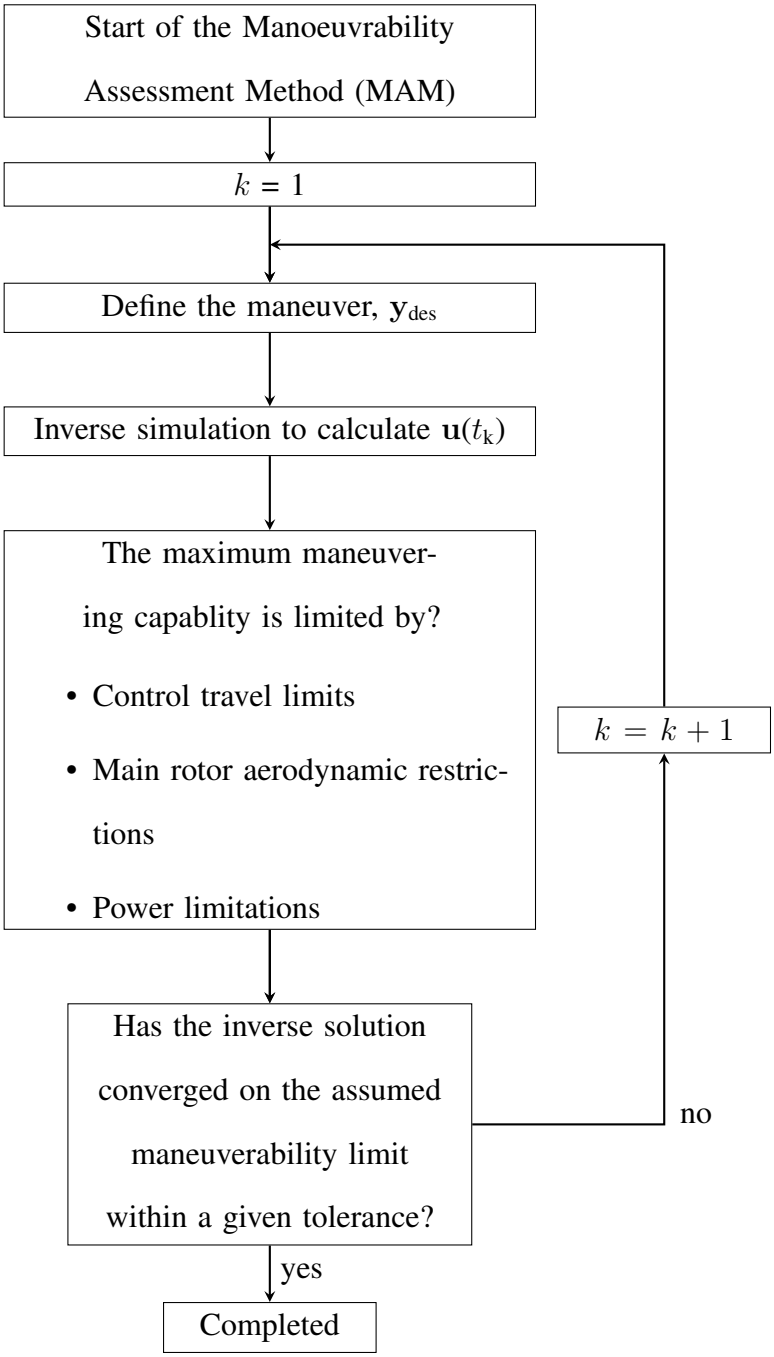

Fig. 5 Flowchart Describing the Maneuverability Assessment Method.

configuration along the desired flight path. With the controls and states calculated throughout the maneuver, the assumed limiting factor determining the vehicle's maneuverability can be calculated. If the limit is selected to be the aerodynamic restrictions of the main rotor then the main rotor blade loading at every time point is calculated. If $C_T/\sigma < (C_T/\sigma)_{max}$ at any time point throughout the maneuver then the aggressiveness of maneuver is redefined until this condition is satisfied. Conversely, if the power available is the limiting factor then the total power throughout the maneuver is calculated and then the maneuver is redefined until MAM converges towards a solution. In terms of the Pullup-Pushover maneuver, the variable n_{max} in the maneuver definition, is allowed to alter the aggressiveness of the maneuver and therefore converge towards the maneuverability limit, whereas with the Accel-Decel maneuver, the distance traveled by the vehicles, S, is varied to converge towards a solution. The maneuverability limit is generally reached within 5 iterations.

Results

ADS-33 Pullup-Pushover Results

With the methodology developed, MAM can now be used to predict the maneuverability of the two aircraft configurations. For both configurations, flying the Pullup-Pushover maneuver, it is assumed that the limiting factors are the aerodynamic restrictions of the two main rotors. Hence, throughout the maneuvers the aerodynamic blade loading of the main rotors, C_T/σ, is calculated and the aggressiveness of the maneuver refined until the maximum blade loading is reached. The Pullup-Pushover maneuver begins at an airspeed of 120 kt and as the aircraft climbs, airspeed begins to reduce due to a gain of potential energy. The maximum blade loading is likely to occur at 3s into the maneuver, since this is where the highest load factor is to be obtained with the lowest amount of translational kinetic energy due to the reduction in the aircraft's speed. At this flight condition the flight speed drops to $\approx$100 kt, which corresponds to an advance ratio, μ, of approximately 0.22. With the use of Figure 4, which approximates a transient maneuver boundary, the maximum blade loading, $(C_T/\sigma)_{max}$, which can be expected at this flight speed is 0.17. As a consequence, it is assumed that the limiting factor for this maneuver is when $(C_T/\sigma)_{max} = 0.17$ for both aircraft configurations.

Figure 6(a) presents the blade loading values at each time point for both aircraft configurations. As expected, the predicted limiting state of the main rotors of the BL and CH configurations occur at ≈3s. It is interesting to the note the large differences in blade loading between the two configurations in the early stages of the maneuver. For example, for the BL configuration, $C_T/\sigma = 0.142$ at 1s, whereas at the same time the CH configuration's blade loading is 0.08. The difference is due the wing offloading the main rotor significantly in the early stages of the maneuver. However, there is a sharp rise in blade loading for the CH configuration between 1-3s as the lifting capability of the wing deteriorates due to loss of dynamic

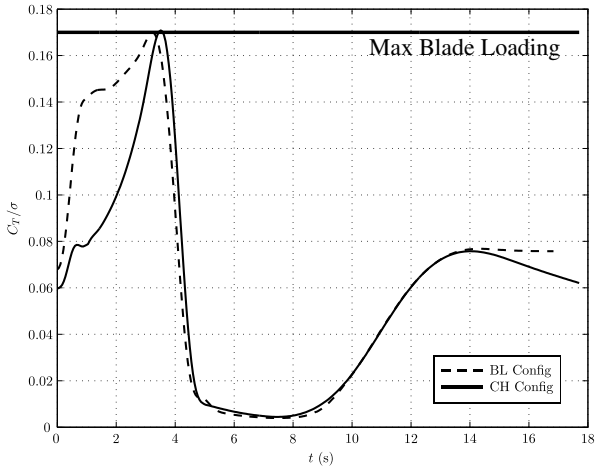

(a) Blade Loading

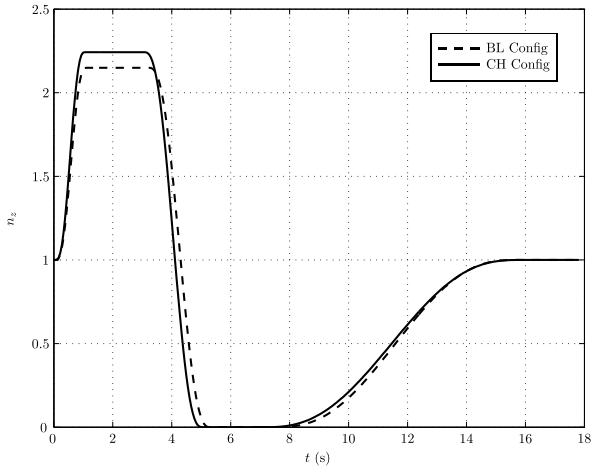

(b) Load Factor Distribution

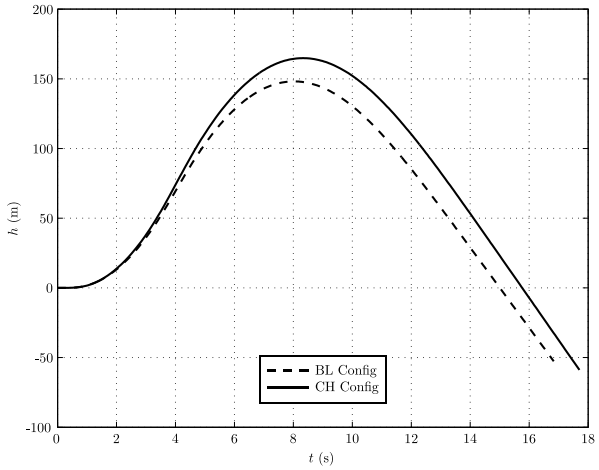

(c) Height Profile

Fig. 6 Flight path during the Pullup-Pushover Maneuvers.

pressure as the vehicle's airspeed reduces. The load distributions achieved by each vehicle are shown in Figure 6(b). The maximum load factors achieved by the CH and BL configurations are 2.243 and 2.149, respectively. As a consequence the CH configuration climbs to a greater height than the BL configuration, with the height profiles of the two configurations shown in Figure 6(c). The CH configuration reaches a height of 164m after 8.5s whereas the BL configuration's maximum height is 147m is attained at 8.2s. Although the CH configuration is capable of climbing to greater height than the BL configuration, the result may be viewed as somewhat surprising as one might intuitively think that the maximum load factor capability of a winged helicopter would significantly surpass the conventional helicopter's capability. This may indeed prove to be the case for high speed maneuvers when the lifting capability of the wing is fully exploited. Figure 7 presents the airspeed and the wing's angle of attack variation throughout the Pullup-Pushover Maneuver. Figure 7 confirms that an effort is made to ensure that the Pullup-Pushover maneuver is flown in a manner which realizes the lifting potential of the wing. For example, Figure 7(a) shows the wing's angle of attack increases significantly in the early stages of the pullup to increase the wing's lifting force, however after 1.5s the wing's angle of attack reduces as the vehicle's airspeed reduces, Figure 7(b). At 3s when the main rotor's blade loading is at its highest, the wing's angle of attack is approximately 10°. This angle of attack promotes a lifting force and as a consequence the wing does produce a contribution

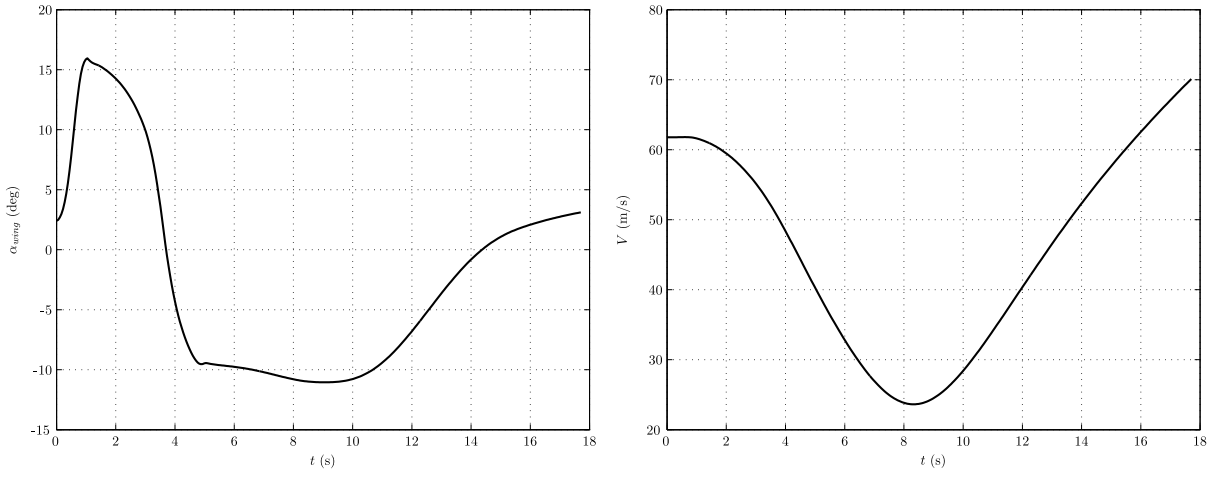

(a) Wing Angle of Attack (b) Airspeed

Fig. 7 Airspeed and Wing's Angle of Attack Variation throughout the Pullup-Pushover Maneuver.

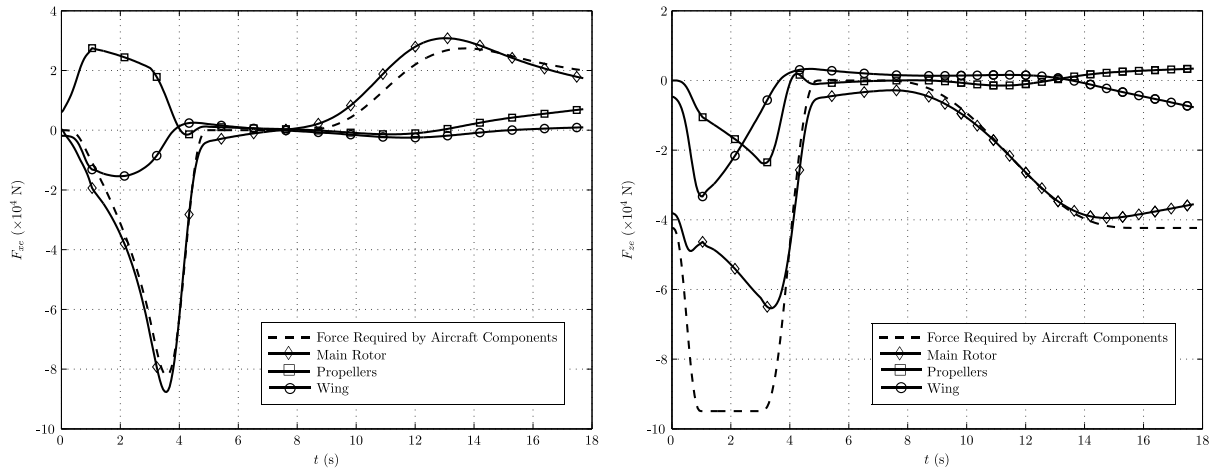

(a) Forces in the x_e axis (b) Forces in the z_e axis

Fig. 8 Main Rotor, Wing and Propeller Forces of the CH Configuration in the x_e and z_e directions of the Earth Axes set during the Pullup-Pushover Maneuver.

to the vertical force to attain the required normal load factor. However, the magnitude of the lifting force is ultimately limited by the relatively low dynamic pressure across the wing. Recall that this maneuver begins at 120 kt which is a modest flight speed for a fixed wing aircraft. Hence, the lifting capability of the wing throughout the maneuver is restricted due to the relatively low airspeeds, particularly after 2s when the CH configuration achieves a high rate of climb, thereby decelerating the aircraft.

To properly interpret the results presented above it is convenient to inspect the forces that the CH configuration's components produce. Figure 8 shows the main rotor, wing and propeller forces in the x_e and z_e directions of the Earth Axes set. Also shown in Figure 8 are the forces required by the aircraft components to complete the maneuver. Note that the forces produced by the fuselage, tailplane and fin are not shown for the purposes of clarity. The pullup stage of the maneuver is characterized by a reduction in airspeed as there is drop a of translational kinetic energy as the aircraft climbs. As a consequence, a significant amount of force in the negative x_e direction is required, as seen in Figure 8(a), by the aircraft components to decelerate the vehicle. Figure 8(a) shows that the main rotor provides the majority of the force to decelerate and pitch the aircraft's nose up in the first part of the maneuver. At 2.5 seconds into the maneuver the wing provides 17kN in the negative x_e direction due to the aircraft's nose pitching

up to attain the necessary load factor. In contrast, the two propellers provide a significant force in the positive x_e direction to overcome the airframe's drag and to maintain the required fuselage angle of attack. Figure 8(b) presents the forces required by the CH configuration's components to provide the required vertical acceleration. In the early stages of the maneuver, upto 1s, the wing's lifting force sharply increases as the aircraft's nose pitches up, thereby increasing the wing's angle of attack. However, after 1s, the wing's lifting force in the z_e direction begins to deteriorate as the aircraft's airspeed begins to reduce as the vehicle climbs. As the result, the lifting force of the wing in the z_e direction at 3s is approximately 9kN. The reduction of the wing's lifting capability is met with an increase in rotor thrust to maintain the required vertical acceleration. It is also interesting to note that the propellers contribute significantly to provide the required normal load factor, with the propellers providing 23kN of useful force in negative z_e direction at 3.5s into maneuver. At this time the vehicle's fuselage pitch angle is approximately 44° . Propellers generally create the majority of their propulsive thrust in the direction normal to the propeller disk plane, however due to the high fuselage pitch angle a significant amount of the propeller's propulsive force transforms into the z_e direction, thereby providing a useful force to obtain the highest load factor possible.

Although not a primary aim of this study, it is worthwhile exploring the pilot inputs to complete the relevant maneuvers. Figure 9 shows the predicted control displacements throughout the maximum Pullup-Pushover maneuvers. In the first second of the maneuver, a large main rotor collective control input is required by the BL configuration to transition to a positive load factor. However, the collective stick of the CH configuration drops within the early stages of the maneuver as the wing provides a significant lifting force, as seen in Figure 8(b). There is also a large initial longitudinal stick input, stick backwards, to pitch the CH configuration's nose up thereby increasing the lifting force provided by the wing. In addition, there is a rapid rise in the mean propeller pitch setting, $\bar{\theta}_{prop}$, within the first second of the initial control input to increase the propulsive force of the two propellers. Therefore, initially the required rotor thrust of the CH configuration is less than that of the BL configuration, consequently lowering the main rotor collective input required. After 4s the trend of the longitudinal stick displacements are similar for the two aircraft configurations. As the vehicles transition to their minimum load factors, n_{min}, both assumed to be 0, the main rotor collective levers drop to lower the level of rotor thrust. The longitudinal cyclic of the

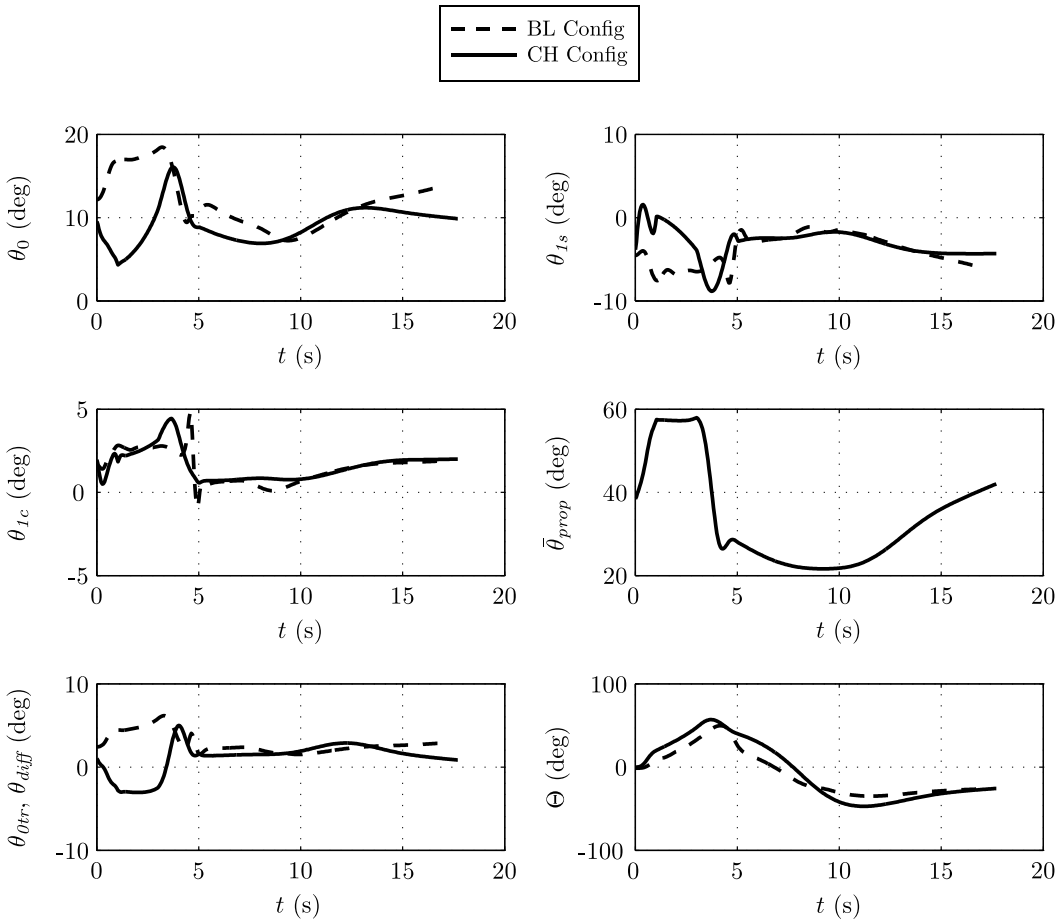

Fig. 9 Maximum Maneuverability Control time histories of the CH and BL configurations during the Pullup-Pushover maneuver.

BL configuration reaches its minimum value at 5s as it pitches down the aircraft to achieve a zero normal load factor. The propeller pitch control input is fairly constant between 1-3s as the CH configuration sustains its positive load factor. However, as the aircraft transitions to a pushover the control input reduces significantly from 56° to a value of 31°. The control remains within this region until it is increased in the latter stages of the maneuver to recover the vehicle's original airspeed. Note that the additional constraint featured in the CH configuration's output vector, chosen to be the fuselage angle of attack, results in a more gradual change of pitch attitude when compared to the BL configuration.

ADS-33 Accel-Decel Results

For the Accel-Decel maneuver, the power available is assumed to be the limiting factor influencing the maneuverability of the two aircraft configurations. Recall that the maneuver capability in low speed flight is generally limited to excess power, as seen in Figure 4. This was confirmed by running the maneuverability assessment method and subsequently checking which limit was breached first. As expected, the power limit was reached before the assumed aerodynamic limit of the main rotor. Figure 10 shows the power variation of the two configurations throughout the maximum Accel-Decel maneuver. The two configurations reach their limiting states, i.e. $P_{tot} = P_{av}$, at the point of maximum forward acceleration, highlighting that MAM has successfully found a solution. Note that it is assumed that the installed engine power of the CH configuration is 2000kW, which is a significant increase from the 1300kW available for the BL configuration. Although this is not a design study, various other studies have concluded that the compound helicopter is expected to have significantly more power than a conventional helicopter [49, 50].

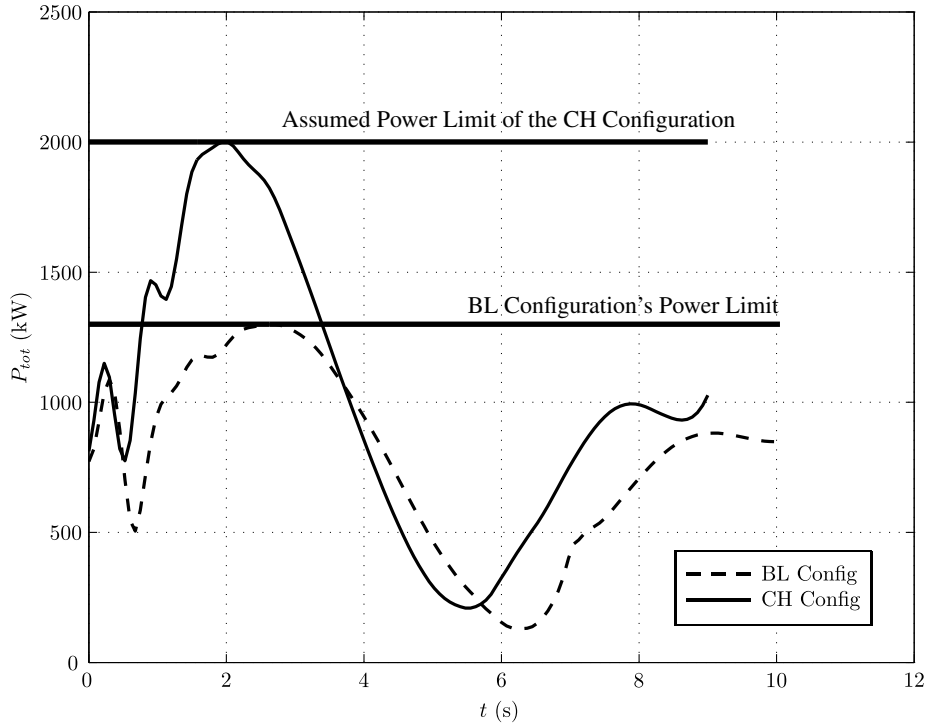

Fig. 10 Power variation of the two configurations throughout the maximum Accel-Decel maneuver.

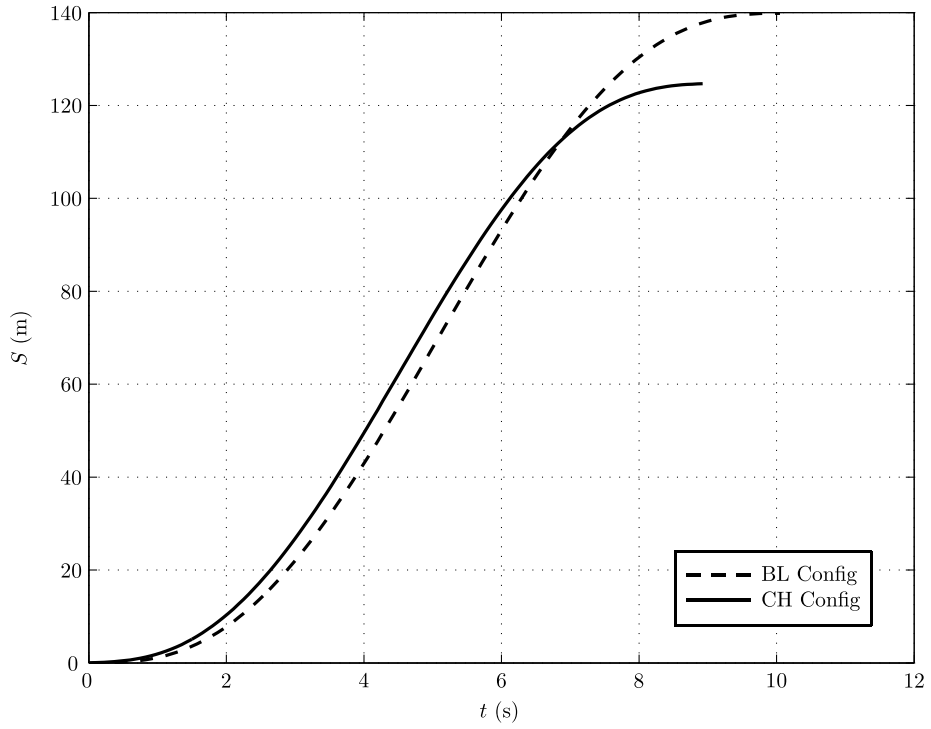

Fig. 11 Flight path of the Maximum Accel-Decel Maneuvers.

The compound helicopter is expected to operate in the high speed range where parasite drag, which is proportional to the cube of the airspeed, dominates the power required [47]. To overcome this parasite power penalty requires a significant reduction of airframe drag or a large increase of installed power. Although it is the goal of the designer to minimize drag there is a practical limit to which the rotorcraft's drag can be reduced. The result is that an increase of installed engine power for the compound helicopter configuration is required. Therefore, in the context of this study, it seems reasonable to increase the CH configuration's available power to assess the vehicle's potential maneuverability. The predicted result is that the CH configuration is capable of completing the maneuver quicker than the BL configuration, as seen in Figure 11, with the BL and CH configurations completing the maneuver in 8.9s and 10.1s, respectively. Figure 11 also shows the longitudinal distance traveled by the two vehicles, with the BL configuration completing the maneuver over a distance of 139.8m, whereas the CH configuration covers a total distance of 124.7m. The end result suggests that the CH configuration is capable of completing the maneuver quicker than the BL configuration at the expense of greater installed power for the CH configuration.

Figure 12 shows the forces produced by CH configuration's main rotor, wing and propellers in the x_e and z_e directions of the Earth Axes set during the Accel-Decel maneuver. Recall that with the CH configuration, the additional constraint imposed in the Accel-Decel maneuver is the amount of propeller thrust that provides the total propulsive force required throughout the maneuver. As expected, the two propellers provide 75% of the total propulsive force at the point of maximum forward acceleration, as seen in Figure 12(a). As the aircraft begins decelerating, the main rotor disk flaps backwards to slow the aircraft's flight speed. As the propellers provide 25% of the required reverse force, at the point of maximum deceleration, the CH configuration decelerates by traditional helicopter maneuvering, by the main rotor disk flapping backwards with the consequence of significantly pitching the vehicle's nose upwards. In terms of the forces in the z_e direction, the vertical force required by the aircraft components is simply the aircraft's weight, as the vehicle does not change height throughout the maneuver. Figure 12(b) presents the forces produced by the aircraft components of the CH configuration in the z_e axis. As seen in Figure 12(b), the main rotor rotor provides the majority of the lifting force throughout the maneuver. The addition of lift compounding to the CH configuration's design is detrimental in this particular maneuver as the wing produces an aerodynamic download throughout the maneuver, Figure 12(b). Although the wing is beneficial at high speeds, to offload the main rotor, in the hover and low speed flight it provides a significant download reducing low speed performance. It is likely that a winged compound helicopter would implement the use of flaps which were used on the tilt-rotor aircraft [51]. However, even with the use of flaps, the wing will still provide an aerodynamic download in the low speed flight, which is an inevitable consequence of lift compounding.

Figure 13 presents the control time histories throughout the maximum Accel-Decel maneuvers. As noted previously, there are five maneuver constraints which are the three accelerations, heading rate and the contribution of the thrust from the two propellers which make up the total propulsive force required. The inverse simulation algorithm calculates the control activity required for the aircraft to fly the maneuver in this particular manner. The advantage of using this fifth constraint is that the two propellers are actively used to provide the majority of propulsive force in the early stages of the maneuver. As a consequence, the two propellers provide 75% of the total force in the x_e axis, as seen in Figure 12(a), at the time where maximum forward acceleration is required. Therefore, the mean propeller pitch, $\bar{\theta}_{prop}$, increases

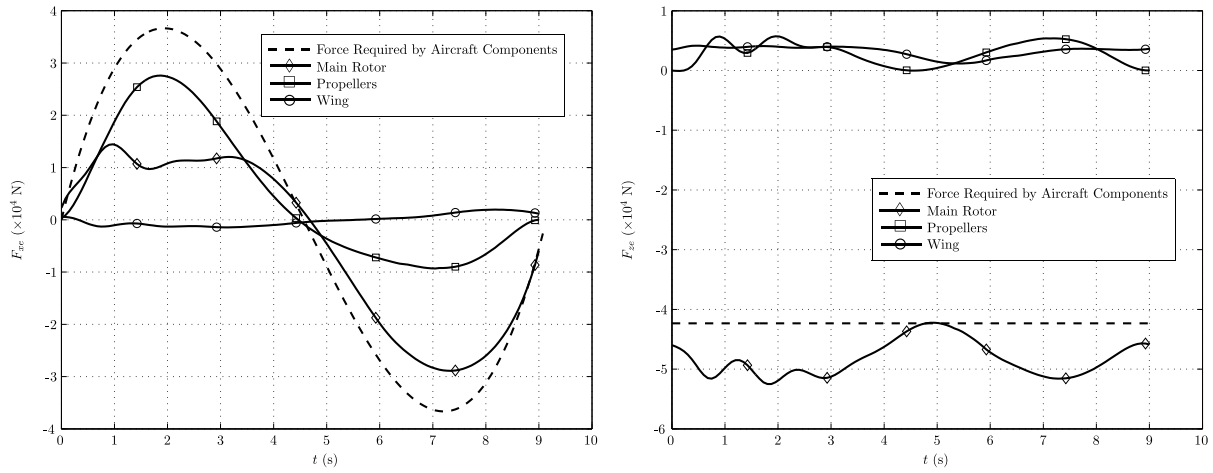

(a) Forces in the x_e axis (b) Forces in the z_e axis

Fig. 12 Main Rotor, Wing and Propeller Forces of the CH Configuration in the x_e and z_e directions of the Earth Axes set during the Accel-Decel Maneuver.

significantly in the early stages of the maneuver, as seen in Figure 13. The trend of $\bar{\theta}_{prop}$ is similar to that of the propulsive force required by the propellers throughout the maneuver, with the control increasing in the first stage of the maneuver and reducing to provide some level of reverse thrust. At the starting position of the maneuver the main collective of the CH configuration is greater than that of the BL configuration. This is due to the wing of the CH configuration providing an aerodynamic download which requires additional collective input to offset the download force. As the maneuver commences, the main rotor collective of the BL configuration increases, to increase rotor thrust, with the control reaching its highest value at 4s. With the CH configuration its highest collective setting is lower than that of the BL configuration. The main rotor is only required to provide 25% of the forward force in the x_e direction, at the time of peak forward acceleration, which consequently reduces the amount of collective input required. For a conventional helicopter the main rotor is responsible for both the propulsive and lifting capability of the vehicle [46]. One undesired quality of the helicopter is that in order to accelerate or decelerate a large pitch excursion is required. Due to the addition of thrust compounding, after 2s the main rotor disk of the CH configuration does not have to tilt as much as the BL configuration in order to provide the propulsive force to accelerate the vehicle. The net effect is that the pitch attitude is reduced, between 1-4s, when the pitch

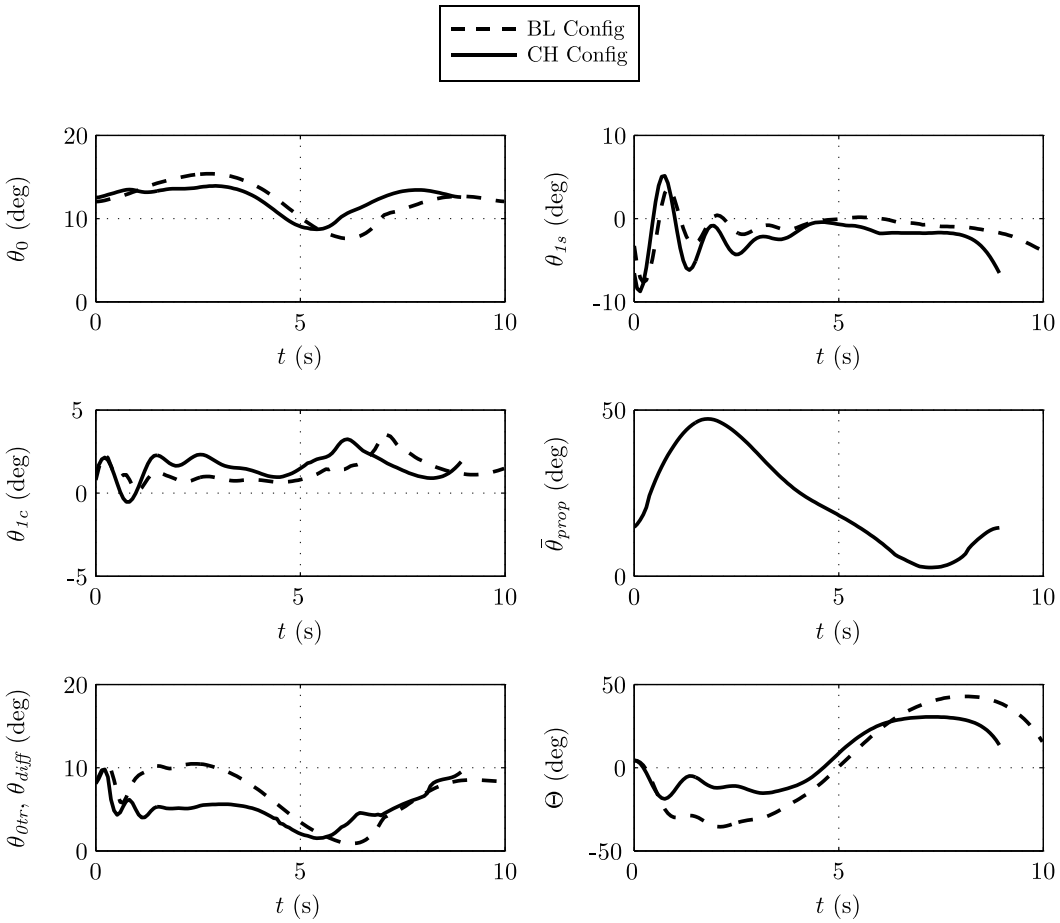

Fig. 13 Maximum Manoeuvrability Control time histories of the CH and BL configurations during the Accel-Decel maneuver.

attitudes of the two configurations are compared, highlighting one of the benefits of thrust compounding. As the propellers provide a modest level of reverse thrust, the CH configuration decelerates by traditional helicopter maneuvering. However, the peak pitch attitude of the CH configuration is lower than that of the BL configuration, as a result of the reverse thrust the two propellers provide. The main rotor cyclic inputs are very similar throughout the maneuver. Both configurations exhibit large oscillatory longitudinal cyclic control inputs at the beginning of the maneuver. In terms of the anti-torque controls, θ_{0tr} and θ_{diff}, their control time histories are similar to the collective settings in order for the aircraft configurations to retain a constant heading.

Conclusions

A preliminary maneuverability assessment of a compound helicopter has been conducted. The paper has predicted the maximum maneuvering capability of a conventional and compound helicopter. In addition, the paper examined some of the likely control strategies a pilot may adopt when flying a compound helicopter. In terms of the Pullup-Pushover maneuver, it is predicted that the compound helicopter is capable of reaching a higher load factor than its conventional counterpart. It is predicted that the CH and BL configurations attain maximum load factors of 2.243 and 2.149, respectively. Therefore, the CH configuration climbs to a maximum height of 164m whereas the BL configuration is capable of climbing to 147m. Although an effort is made to exploit the lifting capability of the wing, the magnitude of the lifting force of the wing is limited by the relatively low flight speeds in which this maneuver is performed. Once the CH configuration initiates the pullup stage of the maneuver then the aircraft's airspeed begins to reduce, lowering the dynamic pressure across the wing, thereby limiting the amount of lifting force the wing can produce. The propellers have a favorable contribution in this maneuver as they supplement the wing and main rotor to achieve the required vertical acceleration, and therefore normal load factor. Concerning the control action required to fly this maneuver, the main rotor collective of the CH configuration is much less than that of the BL configuration, in the initial stages of the maneuver. This is due to the wing providing a significant lifting force in the early stages of the maneuver, upto 1s, before the lifting capability of the wing begins to deteriorate due to the reduction of the vehicle's airspeed. In addition, the introduction of the additional constraint, $\dot{\alpha}$, to calculate the control displacements of the CH configuration, results in significant propulsive force from the propellers to maintain the required fuselage angle of attack. Consequently, the mean propeller setting of the two propellers rises sharply after the initial control inputs.

Regarding the maneuverability of the two configurations flying the Accel-Decel maneuver, it is estimated that the CH configuration is able to complete the maneuver in a shorter distance than the conventional helicopter. The CH configuration is able to complete the maneuver over a distance of 124.7m, compared to 139.8m required by the BL configuration. This highlights one of the potential advantages of thrust compounding but it was noted that more installed engine power is required to achieve this. The

CH configuration is able to complete the forward acceleration stage of the maneuver with the propellers providing the majority of axial force. The addition of thrust compounding lowers the required pitch attitude of the vehicle in the forward acceleration stage of the maneuver as the main rotor does not have to provide a significant propulsive force. As a result, the tilt of the rotor disk is smaller than that of the BL configuration, attenuating the pitch attitude. In contrast, the deceleration phase of the maneuver is carried out using a more traditional helicopter maneuvering strategy as it is assumed that two propellers provide only 25% of the decelerating force, at the point of maximum deceleration. Hence, the main rotor disk is required to flap backwards to provide the force to the decelerate the aircraft. The cyclic control activity of the two configurations is similar throughout the maneuver.

Acknowledgments

The authors would like to acknowledge the Scottish Funding Council (SFC) for providing the funding, under the GRPE Scholarship, to conduct this research.

References

[1]Orchard, M., and Newman, S., "The compound helicopter - why have we not succeeded before?" *The Aeronautical Journal*, Vol. 103, (1028), 1999, pp. 489–495.

[2]Thomson, D., and Bradley, R., "Inverse simulation as a tool for flight dynamics research - Principles and applications," *Progress in Aerospace Sciences*, Vol. 42, (3), May 2006, pp. 174–210.
doi: 10.1016/j.paerosci.2006.07.002

[3]Thomson, D., and Bradley, R., "An analytical method of quantifying helicopter agility," Proceedings of the 12th European Rotorcraft Forum, 1986.

[4]Thomson, D., and Bradley, R., "An investigation of pilot strategy in helicopter nap-of-the-earth manoeuvres by comparison of flight data and inverse simulation," Royal Aeronautcal Society: helicopter handling qualities and control, 1988.

[5]Thomson, D., and Bradley, R., "The use of inverse simulation for conceptual design," 16th European Rotorcraft Forum, 1990.

[6]Thomson, D., and Bradley, R., "The use of inverse simulation for preliminary assessment of helicopter handling qualities," *The Aeronautical Journal*, Vol. 101, (1007), 1997, pp. 287 – 294.

[7]Cameron, N., Thomson, D., and Murray-Smith, D., "Pilot modelling and inverse simulation for initial handling qualities assessment," *The Aeronautical Journal*, Vol. 107, (1074), 2003, pp. 511– 520.

[8]Hess, R., Gao, C., and Wang, S., "Generalized technique for inverse simulation applied to aircraft maneuvers," *AIAA Journal of Guidance, Control and Dynamics*, Vol. 14, (5), 1991, pp. 920–926.
doi: 10.2514/3.20732

[9]Hess, R., and Gao, C., "A Generalized Algorithm for Inverse Simulation Applied to Helicopter Maneuvering Flight," *Journal of the American Helicopter Society*, Vol. 38, (4), 1993, pp. 3 – 15.
doi: 10.4050/JAHS.38.3

[10]Avanzini, G., de Matteis, G., and de Socio, L., "Two-Timescale-Integration Method for Inverse Simulation," *Journal of Guidance, Control and Dynamics*, Vol. 22, (3), 1999, pp. 395–401.
doi: 10.2514/2.4410

[11]Avanzini, G., and de Matteis, G., "Two-timescale inverse simulation of a helicopter model," *Journal of Guidance, Control and Dynamics*, Vol. 24, (2), 2001, pp. 330–339.
doi: 10.2514/2.4716

[12]Celi, R., "Optimization-Based Inverse Simulation of a Helicopter Slalom Maneuver," *Journal of Guidance, Control and Dynamics*, Vol. 23, (2), 2000, pp. 289–297.
doi: 10.2514/2.4521

[13]de Matteis, G., de Socio, L., and Leonessa, A., "Solution of Aircraft Inverse Problems by Local Optimization," *AIAA Journal of Guidance, Control and Dynamics*, Vol. 18, (3), 1995, pp. 567–571.
doi: 10.2514/3.21424

[14]Horn, J., Calise, A., and Prasad, J., "Flight Envelope Cueing on a Tilt-Rotor Aircraft Using Neural Network Limit Prediction," *Journal of the American Helicopter Society*, Vol. 46, (1), 2001, pp. 23–31.
doi: 10.4050/JAHS.46.23

[15]Horn, J., Calise, A., and Prasad, J., "Flight Envelope Limit Detection and Avoidance for Rotorcraft," *Journal of the American Helicopter Society*, Vol. 46, (1), 2001, pp. 253–262.
doi: 10.4050/JAHS.46.23

[16]Sahani, N., and Horn, J., "Adaptive Model Inversion Control of a Helicopter with Structural Load Limiting," *Journal of Guidance, Control and Dynamics*, Vol. 29, (2), 2006, pp. 411–420.
doi: 10.2514/1.13391

[17]Rysdyk, R., and Calise, A., "Adaptive Model Inversion Flight Control for Tiltrotor Aircraft," American Helicopter Society 54th Annual Forum, 1998.

[18]Kim, B., and Calise, A., "Nonlinear Flight Control Using Neural Networks," Proceedings of the AIAA Guidance, Navigation and Control Conference, 1994.

[19]Leitner, J., Calise, A., and Prasad, J., "Analysis of Adaptive Neural Network for Helicopter Flight Control," Proceedings of the AIAA Guidance, Navigation and Control Conference1, 1995.

[20]Slotine, J., and Li, W., *Applied Nonlinear Control*, Prentice-Hall, New Jersey, 1991.

[21]Calise, A., and Rysdyk, R., "Nonlinear adaptive flight control using neural networks," *Control Systems, IEEE*, Vol. 18, (6), 1998.
doi: 10.1109/37.736008

[22]Olson, J., and Scott, M., "Helicopter Design Optimization for Maneuverability and Agility," American Helicopter Society 45th Annual Forum, 1989.

[23]Johnson, K., *Prediction of Operational Envelope Maneuverability Effects of Rotorcraft Design*, Ph.D Thesis, Georgia Institute of Technology, 2013.

[24]Levine, L., Warburton, F., and Curtiss Jr, H., "Assessment of Rotorcraft Agility and Maneuverability with Pilot-in-the-loop Similation," American Helicopter Society 41st Annual Forum, 1985.

[25]Whalley, M., "Development and Evaluation of an Inverse Solution Technique for Studying Helicopter Maneuverability and Agility," USAAVSCOM TR 90-A-008, 1991.

[26]Padfield, G., *Helicopter Flight Dynamics: the Theory and Application of Flying Qualities and Simulation Modelling*, Blackwell Publishing, second edition, 2007.

[27]Orchard, M., and Newman, S., "The fundamental configuration and design of the compound helcopter," *Proceedings of the Institution of Mechanical Engineers, Part G: Journal of Aerospace Engineering*, Vol. 217, (6), 2003, pp. 297–315.
doi: 10.1243/095441003772538570

[28]Lentine, F., Groth, W., and Oglesby, T., "Research in Maneuverability of the XH-51A Compound Helicopter," USAAVLABS Technical Report 68-23, 1968.

[29]Ferguson, K., and Thomson, D., "Flight dynamics investigation of compound helicopter configurations," *AIAA Journal of Aircraft*, Vol. 52, (1), 2015.
doi: 10.2514/1.C032657

[30]Thomson, D., "Development of a Generic Helicopter Mathematical Model for Application to Inverse Simulation," Internal Report No. 9216, Department of Aerospace Engineering, University of Glasgow, UK, 1992.

[31]Kim, F., Celi, R., and Tischler, M., "Forward flight trim and frequency response validation of a helicopter simulation model," *AIAA Journal of Aircraft*, Vol. 30, (6), 1993, pp. 854–863.
doi: 10.2514/3.46427

[32]Rutherford, S., *Simulation Techniques for the Study of the Manoeuvring of Advanced Rotorcraft Configurations*, Ph.D Thesis, University of Glasgow, 1997.

[33]Mansur, M., "Development and Validation of a Blade Element Mathematical Model for the AH-64A Apache Helicopter," NASA-TM-108863, 1995.

[34]Houston, S., "Validation of a non-linear individual blade rotorcraft flight dynamics model using a perturbation method," *The Aeronautical Journal*, Vol. 98, (977), 1994, pp. 260–266.

[35]Bradley, R., Padfield, G., Murray-Smith, D., and Thomson, D., "Validation of helicopter mathematical models," *Transactions of the Institute of Measurement and Control*, Vol. 12, (186), 1990.
doi: 10.1177/014233129001200405

[36]Lu, L., Murray-Smith, D. J., and Thomson, D., "Issues of numerical accuracy and stability in inverse simulation," *Simulation Modelling Practice and Theory*, Vol. 16, (9), October 2008, pp. 1350–1364.
doi: 10.1016/j.simpat.2008.07.003

[37]Keys, C., "Performance Prediction of Helicopters," *Rotor-Wing Aerodynamics*, edited by W. Stepniewski, Dover Publications, Inc., 1981.

[38]Torres, M., "A Wing on the SA.341 Gazelle Helicopter and its Effects," *Vertica*, Vol. 1, (1), 1976, pp. 67–73.

[39]Dumond, R., and Simon, D., "Flight Investigation of Design Features of the S-67 Winged Helicopter," *Journal of the American Helicopter Society*, Vol. 18, (3), 1973, pp. 2–9.
doi: 10.4050/JAHS.18.2

[40]Von Mises, R., *Theory of Flight*, Dover Publications, 1959.

[41]Rutherford, S., *Simulation Techniques for the Study of Advanced Rotorcraft*, Phd, University of Glasgow, 1997.

[42]Thomson, D., and Bradley, R., "Mathematical Definition of Helicopter Maneuvers," *Journal of the American Helicopter Society*, Vol. 4, (1), 1997, pp. 307 – 309.
doi: 10.4050/JAHS.42.307

[43]Anon., "Handling qualities requirements for military rotorcraft," Aeronautical design standard ADS-33E-PRF, United States army aviation and troop command, 2000.

[44]Celi, R., "Analytical Simulation of ADS-33 Mission Task Elements," American Helicopter Society 63rd Annual Forum, 2007.

[45]Thomson, D., *Evaluation of helicopter agility through inverse solution of the equations of motion*, Ph.D Thesis, University of Glasgow, 1987.

[46]Leishman, J., *Principals of Helicopter Aerodynamics*, Cambridge University Press, second edition, 2006.

[47]Johnson, W., *Rotorcraft Aeromechanics*, Cambridge University Press, 2013, p. 243.

[48]Lappos, N. and Padfield, G., "Design Helicopters for Agility," AGARD AR-314 Operational Agility, 1994.

[49]Ferguson, K., and Thomson, D., "Performance comparison between a conventional helicopter and compound helicotper configurations," *Proceedings of the Institution of Mechanical Engineers, Part G: Journal of Aerospace Engineering*, 2015.
doi: 10.1177/0954410015577997

[50]Jordan, T., Humpherson, D., and Benger, B., "The compound helicopter - The rotorcraft for the 21st Century?" American Helicopter Society 49th Annual Forum, 1993.

[51]Felker, F., Maisel, M., and Betzina, M., "Full-Scale Tilt-Rotor Hover Performance," *Journal of the*

American Helicopter Society, Vol. 31, (2), 1986, pp. 10–18.

doi: 10.4050/JAHS.31.10

List of Figures

List of Tables